

# Main restrictions in the synthesis of new superheavy elements: quasifission or/and fusion-fission

A. K. Nasirov<sup>1,2</sup>, Kyungil Kim<sup>3</sup>, G. Mandaglio<sup>4,5,6</sup>,  
G. Giardina<sup>4,5</sup>, A. I. Muminov<sup>2</sup>, Youngman Kim<sup>3</sup>

<sup>1</sup>*Joint Institute for Nuclear Research,  
Joliot-Curie 6, 141980 Dubna, Russia*

<sup>2</sup>*Institute of Nuclear Physics,  
Ulugbek, 100214, Tashkent, Uzbekistan*

<sup>3</sup>*Rare Isotope Science Project,  
Institute for Basic Science,  
Daejeon 305-811, Republic of Korea*

<sup>4</sup>*Dipartimento di Fisica e di Scienze della Terra dell' Università di Messina,  
Salita Sperone 31, 98166 Messina, Italy*

<sup>5</sup>*Istituto Nazionale di Fisica Nucleare,  
Sezione di Catania, Italy*

<sup>6</sup>*Centro Siciliano di Fisica Nucleare e  
Struttura della Materia 95125 Catania, Italy*

(Dated: Today)

## Abstract

The synthesis of superheavy elements stimulates the effort to study the peculiarities of the complete fusion with massive nuclei and to improve theoretical models in order to extract knowledge about reaction mechanism in heavy ion collisions at low energies. We compare the theoretical results of the compound nucleus (CN) formation and evaporation residue (ER) cross sections obtained for the  $^{48}\text{Ca}+^{248}\text{Cm}$  and  $^{58}\text{Fe}+^{232}\text{Th}$  reactions leading to the formation of the isotopes  $A = 296$  and  $A = 290$ , respectively, of the new superheavy element Lv ( $Z = 116$ ). The ER cross sections, which can be measured directly, are determined by the complete fusion and survival probabilities of the heated and rotating compound nucleus. That probabilities can not be measured unambiguously but the knowledge about them is important to study the formation mechanism of the observed products. For this aim, the  $^{48}\text{Ca}+^{249}\text{Cf}$  and  $^{64}\text{Ni}+^{232}\text{Th}$  reactions have been considered too. The use of the mass values of superheavy nuclei calculated in the framework of the macroscopic-microscopic model by Warsaw group leads to smaller ER cross section for all of the reactions (excluding the  $^{64}\text{Ni}+^{232}\text{Th}$  reaction) in comparison with the case of using the masses calculated by Peter Möller *et al.*

PACS numbers: 25.70.Jj, 25.70.Gh, 25.85.-w

## I. INTRODUCTION

The heaviest superheavy element which was synthesized in the cold-fusion ( $^{70}\text{Zn}+^{209}\text{Bi}$ ) reaction was  $Z=113$ : it was observed with a cross section of tens femtobarn, *i.e.* 50 fb [1]. The hot fusion reactions were more favorable to synthesis of superheavy elements  $Z=114$ –118 in Joint Institute for Nuclear Research (Dubna, Russia) [2, 3]. As a result, the Mendeleev Table of chemical elements has been extended by new elements Fl ( $Z = 114$ ) and Lv ( $Z = 116$ ) after those experimental results have been certificated in the other experiments devoted to synthesis of elements 114 and 116 in the  $^{48}\text{Ca}+^{244}\text{Pu}$  [4] and  $^{48}\text{Ca}+^{248}\text{Cm}$  [5, 6] reactions, respectively.

The very small cross sections of synthesis of superheavy elements require to find favorable reactions (projectile and target pair) and the optimal beam energy range which is very narrow (no more 10 MeV). It is necessary to establish conditions to increase the events of the ER formation. The experimental way to estimate possibility of the synthesis of the wanted superheavy element is to study yield of fissionlike products and their mass-angle distributions. The presence of the mass-symmetric or around mass-symmetric binary reaction products and their isotropic angular distribution is a necessary condition. The compound nucleus (CN) formation must survive against fission to be registered as the evaporation residue. The fission probability can be very large due to decrease or disappearance of the fission barrier at large values of the excitation and rotational energies of the just formed CN. So, survival probability of the heated and rotating CN against fission is also an important factor which is subject for the further theoretical and experimental studies. Therefore, theoretical studies of the reaction mechanism in collision of massive nuclei and of the range of the favorable beam energy are essential.

The ER formation process is the last stage of the reaction mechanism in heavy ion collisions near the Coulomb barrier energies. The sketch of the preceded stages to formation of the evaporation residues is presented in Fig. 1. Naturally, the threshold interaction of projectile and target nuclei ending with the ER formation begins with the multinucleon transfer reactions. We should distinguish two kinds of reactions which are in competition during heavy ion collisions at low (near the Coulomb barrier) energies of the projectile. The first one is deep-inelastic collisions and the second one is capture reactions shown on the top of Fig. 1. The difference between capture and deep-inelastic collision is whether a path

of the relative motion has been trapped into the well of the nucleus-nucleus interaction or not (see Fig. 2). In the case of capture the full momentum transfer takes place, while it does not in the deep-inelastic collisions (I-channel of binary reaction in heavy ion collisions, see Fig. 1). In both cases the dinuclear system (DNS) will be formed. The lifetime of DNS formed in the capture process will be sufficiently long. Two conditions must be satisfied for capture: 1) the initial energy  $E_{\text{c.m.}}$  of projectile in the center-of-mass system should be sufficiently large to overcome the interaction barrier (Coulomb barrier + rotational energy of the entrance channel), 2) some part of the relative kinetic energy have to be dissipated in order that DNS would be trapped in the well of the nucleus-nucleus interaction potential [7]. If there is not a potential well the deep-inelastic collision takes place only. Here we state that mass distributions of the deep-inelastic collision and capture reaction (quasifission) products may overlap in reactions with nuclei having magic proton or/and neutron numbers [8]. In this case, usually, the contribution of quasifission is arrogated to the deep-inelastic collision.

The capture is the first step in the way to ER formation, and it leads to formation of a molecule-like DNS which can evolve by changing its charge and mass asymmetry due to multinucleon transfer and by changing its shape. The angular velocity of the rotating DNS depends on the initial value of orbital angular momentum which is determined by the impact parameter  $b$  and momentum  $P$  of the collision:  $|\vec{L}| = \vec{\ell}\hbar = |[\vec{b} \times \vec{P}]|$ .

The study of dynamics of the heavy ion collisions near the Coulomb barrier energies showed that complete fusion does not occur immediately in the case of massive nucleus collisions [9–12]. Evolution of DNS may end with the CN formation in the equilibrium state or may arrive at two fragments without reaching the CN state. Quasifission takes place when DNS prefers to break down into two fragments instead of being transformed into fully equilibrated CN.

For example, the total kinetic energy of the quasifission fragments is close to that of fission fragments. The mass and angular distributions of the fragments depend on the entrance channel properties and may overlap, causing difficulties in identification of a mechanism which produces the corresponding reaction products [13]. We should stress the dominant role of the quasifission channel in reactions with massive nuclei that causes strong hindrance to the formation of CN during the evolution of DNS. This important topic will be discussed in the present paper.

Mononucleus survived against quasifission can reach equilibrium shape, and it may be

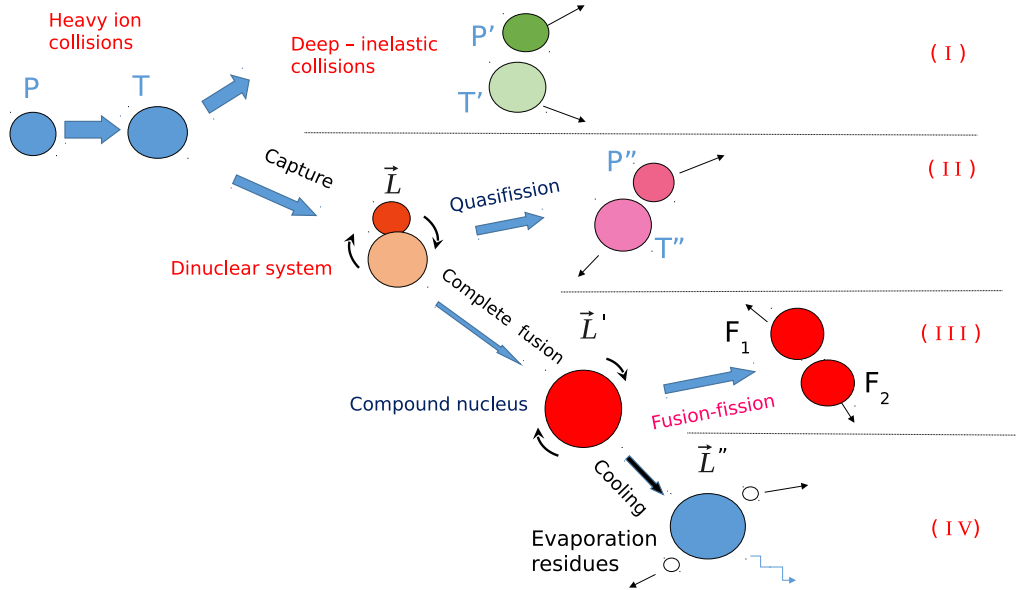


FIG. 1: (Color online) The sketch of the damped reaction channels (I-III) leading to formation of binary or fissionlike fragments which compete in the way to complete fusion (IV) of the initial projectile P and target T nuclei: P' and T' are deep-inelastic collision (not full momentum transfer) products; P'' and T'' quasifission (full momentum transfer) products; F<sub>1</sub> and F<sub>2</sub> are fusion-fission fragments.

transformed into CN. The heated and rotating CN must survive against fission to be registered in a detector as the recoil nucleus through de-excitation by emission of neutrons, protons,  $\alpha$ -particles, and gamma-quanta. The fusion-fission forms binary fragments (the channel (III) in Fig. 1). This fusion-fission channel can be enriched by the fast fission products. Fast fission, which requires no fission barrier, is splitting of mononucleus before reaching equilibrated CN. The properties of fission barrier can be described by liquid drop model for the intermediate mass and heavy nuclei. The stability of very heavy atomic nuclei with charge number  $Z > 106$  against fission appears only due to shell effects in their binding energy [14, 15], which is sensitive to the  $\ell$  and  $E_{CN}^*$  values. Fission barrier of nucleus related with both nature (liquid drop and shell effect) disappears at large values of angular momentum  $L$  [16] and when shell effects have been completely damped [17] as a function of the excitation energy and angular momentum. The increase of the angular momentum leads to damping of the shell effects and a mononucleus which has survived against quasifission can not reach CN equilibrium shape and suffers fast fission. At last, the CN, which survived

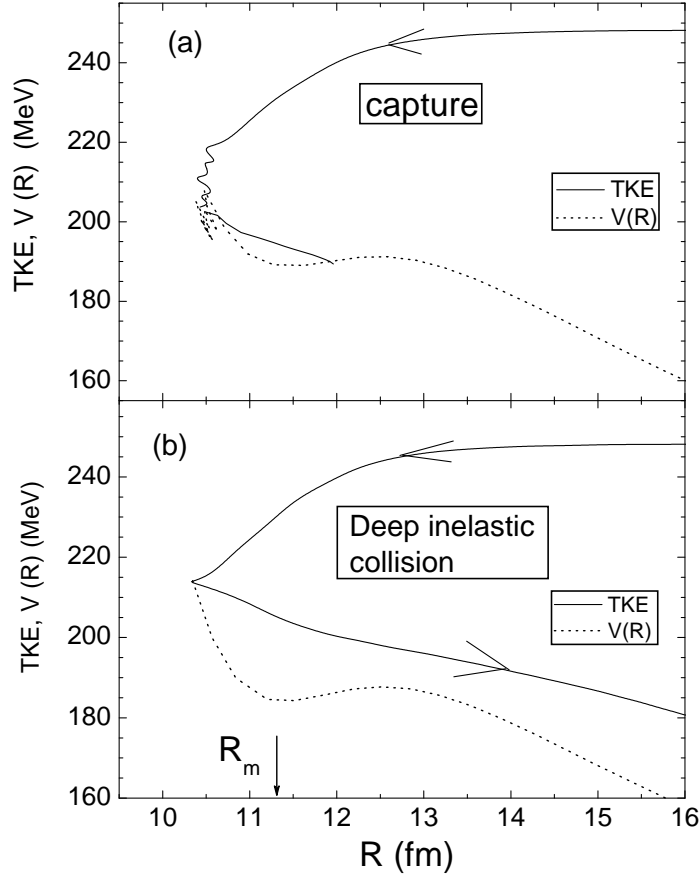


FIG. 2: (Color online) Illustration of capture (a) and deep inelastic collision (b) at heavy ion collisions. Total kinetic energy (TKE) of the relative motion and the part of nucleus-nucleus potential are shown by solid and dotted curves, respectively.

against fission by emission of particles during its cooling, forms the ER which is a product of channel (IV) in Fig. 1.

The main scope of this work is to reproduce the measured data for the superheavy elements with  $Z = 116$  and  $Z = 118$  formed in the  $^{48}\text{Ca}+^{248}\text{Cm}$  and  $^{48}\text{Ca}+^{249}\text{Cf}$  reactions, respectively, and to make predictions for  $\sigma_{\text{ER}}$  in the  $^{58}\text{Fe}+^{232}\text{Th}$  and  $^{64}\text{Ni}+^{232}\text{Th}$  reactions which can be used in future experiments.

The dynamics of heavy ion collisions at low energies is determined by the peculiarities of the nucleus-nucleus interaction. The landscape of potential energy surface (PES)  $U$  plays a main role to estimate the complete fusion probability in competition with quasifission. It is calculated as a sum of the reaction energy balance ( $Q_{\text{gg}}$ ) and the nucleus-nucleus potential ( $V(R)$ ) between interacting nuclei:

$$U(Z, A, \ell, R) = Q_{\text{gg}} + V(Z, A, R, \ell), \quad (1)$$

where  $Z = Z_1$  and  $A = A_1$  are charge and mass numbers of a DNS fragment while the ones of another fragment are  $Z_2 = Z_{\text{tot}} - Z_1$  and  $A_2 = A_{\text{tot}} - A_1$ , where  $Z_{\text{tot}}$  and  $A_{\text{tot}}$  are the total charge and mass numbers of a reaction, respectively;  $Q_{\text{gg}}$  is the reaction energy balance used to determine the excitation energy of CN:  $Q_{\text{gg}} = B_1 + B_2 - B_{\text{CN}}$ . The binding energies the initial projectile and target nuclei ( $B_1$  and  $B_2$ ) are obtained from the mass tables in Ref. [19], while the one of CN ( $B_{\text{CN}}$ ) are obtained from the mass tables [20, 26] The use of nuclear binding energies including shell effects in the PES and driving potential of DNS leads to the appearance of hollows on the PES around the charge and mass symmetries corresponding to the constituents of DNS with the magic proton or/and neutron numbers (see Figs. 3 and 4).

The driving potential  $U_{\text{dr}}(Z, R_m)$  is shown by the broken dot-dashed line in Fig. 3 and it is determined by the minimum values of the potential wells for each charge value  $Z$ . The position of the minimum value of interaction potential on the relative distance is denoted as  $R_m$ . The values of  $U_{\text{dr}}(Z, R_m)$  as a function of angular momentum  $\ell$  are found from the data of PES calculated by formula

$$U_{\text{dr}}(Z, A, \ell, R_m) = Q_{\text{gg}} + V(R, \ell) = B_1 + B_2 - B_{\text{CN}} + V(Z, A, R_m, \ell). \quad (2)$$

If there is no potential well of  $V(Z, A, R, \ell)$  at large values of angular momentum or for symmetric massive nuclei, we use  $R_m$  corresponding to the smallest value of the derivation  $\partial V(Z, A, R_m, \ell)/\partial R$  in the contact area of nuclei.

Capture stage is shown by arrow (a) in Fig. 3 and one of possibilities of the DNS quasifission is shown by (c), while arrow (b) shows complete fusion direction.

In Fig. 4 we compare the driving potentials calculated for the DNS formed in the  $^{48}\text{Ca}+^{248}\text{Cm}$  and  $^{58}\text{Fe}+^{232}\text{Th}$  reactions which can lead to the formation of compound nucleus with  $^{296}\text{Lv}$  and  $^{290}\text{Lv}$ , respectively, as a function of the fragment charge number. PES and driving potential are function of the orientation angles  $\alpha_1$  and  $\alpha_2$  of interacting nuclei. The figures 3 and 4 have been calculated for the intermediate values of the orientation angles.

It is seen from Fig. 4 that the driving potential decreases abruptly for the fragment with charge number larger than  $Z = 30$  for both the  $^{48}\text{Ca}+^{248}\text{Cm}$  and  $^{58}\text{Fe}+^{232}\text{Th}$  reactions. If the value of the driving potential corresponding to the entrance channel is very low relative to its maximum value in the fusion direction  $Z \rightarrow 0$ , the intrinsic fusion barrier  $B_{\text{fus}}^*$  becomes larger and the hindrance to complete fusion will be very strong. It is determined as a difference

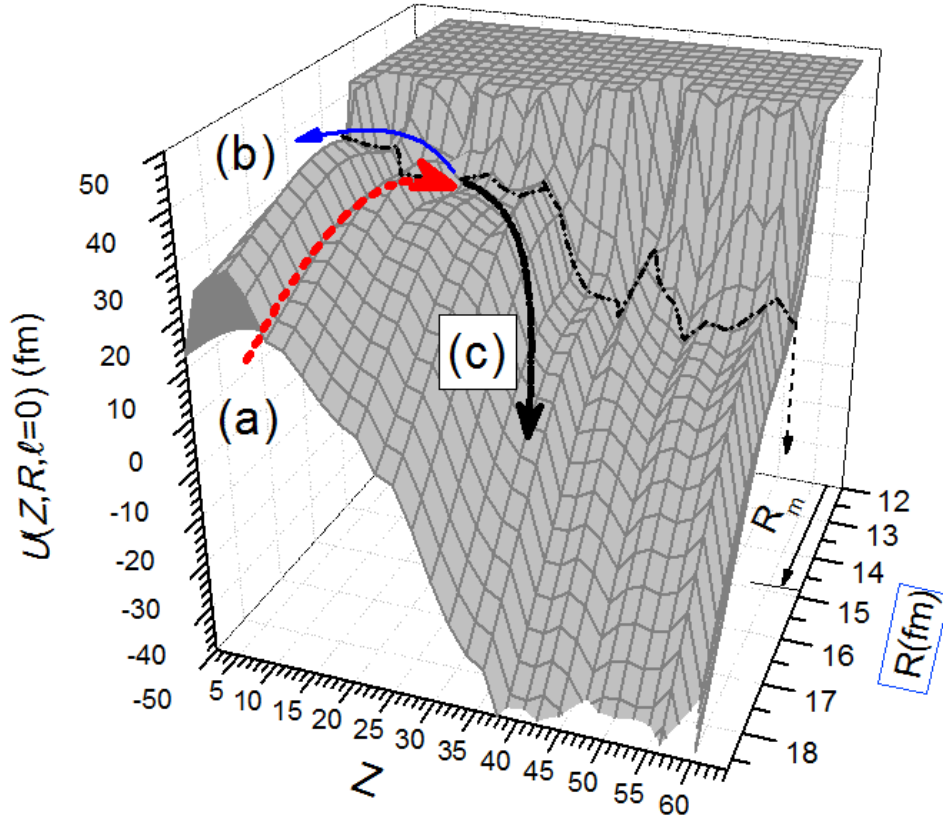


FIG. 3: (Color online) Potential energy surface calculated for the DNS leading to formation of the  $^{296}_{116}$  compound nucleus as a function of the relative distance between the centers of mass of interacting nuclei and mass number of a fragment. The capture stage path is shown by arrow (a) and complete fusion by multinucleon transfer occurs (b) if system overcomes intrinsic fusion barrier. Arrow (c) shows one of possibilities of the DNS quasifission. The broken dot-dashed line corresponds to the driving potential  $U(Z, R_m)$  which is determined by the minimum values of the potential wells for each charge value  $Z$ .  $R_m$  is the position of the minimum value of interaction potential on the relative distance  $R$ .

between the maximum value of the driving potential between  $Z = 0$  and  $Z = Z_P$  and its value corresponding to the initial charge value:

$$B_{\text{fus}}^* = U_{\text{driv}}^{\text{max}} - U_{\text{driv}}(Z_P), \quad (3)$$

where  $U_{\text{driv}}^{\text{max}} = U_{\text{driv}}(Z = 9)$ ;  $Z_P = 20$  and  $Z_P = 26$  for these two reactions under discussion. The values of  $B_{\text{fus}}^*$  are equal to 8.5 MeV and 11.5 MeV for the the  $^{48}\text{Ca}+^{248}\text{Cm}$  and  $^{58}\text{Fe}+^{232}\text{Th}$  reactions, respectively (see Fig. 4).

The mass and charge asymmetry of the entrance channel is enough large in the reactions

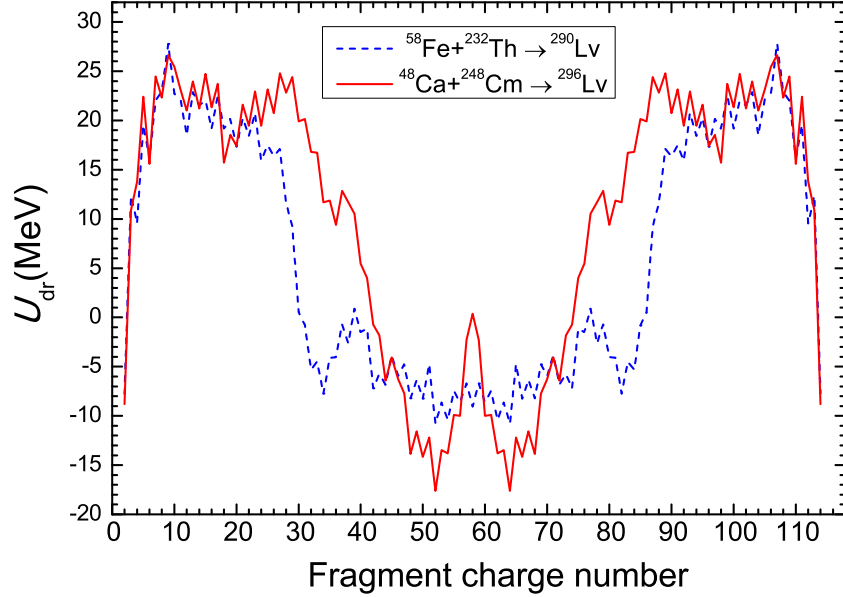


FIG. 4: (Color online) Comparison of the driving potentials calculated for the DNS formed in the  $^{48}\text{Ca}+^{248}\text{Cm}$  and  $^{58}\text{Fe}+^{232}\text{Th}$  reactions which can lead to formation of isotopes  $A=296$  and  $290$  of new superheavy element Lv ( $Z=116$ ) as a function of the fragment charge number.

with  $^{48}\text{Ca}$ -projectile and actinide-targets, and so we deal with hot fusion reactions: a CN is formed with relatively large excitation energy and with large fusion probability. To form DNS with the target nucleus, a projectile must overcome the entrance channel barrier consisting of the Coulomb potential and rotational energy moving along the relative distance  $R$ . As we can see from Fig. 3 the maximum value of PES along the axis  $R$  for the fixed value  $Z = 20$  is larger than the one for the charge asymmetry  $Z = 26$ . Therefore, the large excitation energy of CN is an inevitable circumstance in the hot fusion reactions because after capture and formation of the DNS, the value of PES corresponding to the charge asymmetry of entrance channel is settled at higher points of its hollow in comparison with the case of cold fusion reactions. Therefore, even if the CN is formed by as possible minimum beam energy, it is excited at energies higher than  $E_{\text{CN}}^*=30$  MeV.

The values of the potential energy surface calculated for the  $^{48}\text{Ca}+^{248}\text{Cm}$  reaction corresponding to the initial charge numbers  $Z_P=20$  and  $Z_T=96$  are placed in the valley formed due to shell effects. The (see solid line in Fig. 4). Note that  $^{48}\text{Ca}$  is double magic nucleus ( $Z = 20$  and  $N = 28$ ). As a result there is an intrinsic fusion barrier  $B_{\text{fus}}^*$  which must be overcome by DNS to be transformed into CN.

The capture stage path is shown by arrow (a) and complete fusion by multinucleon

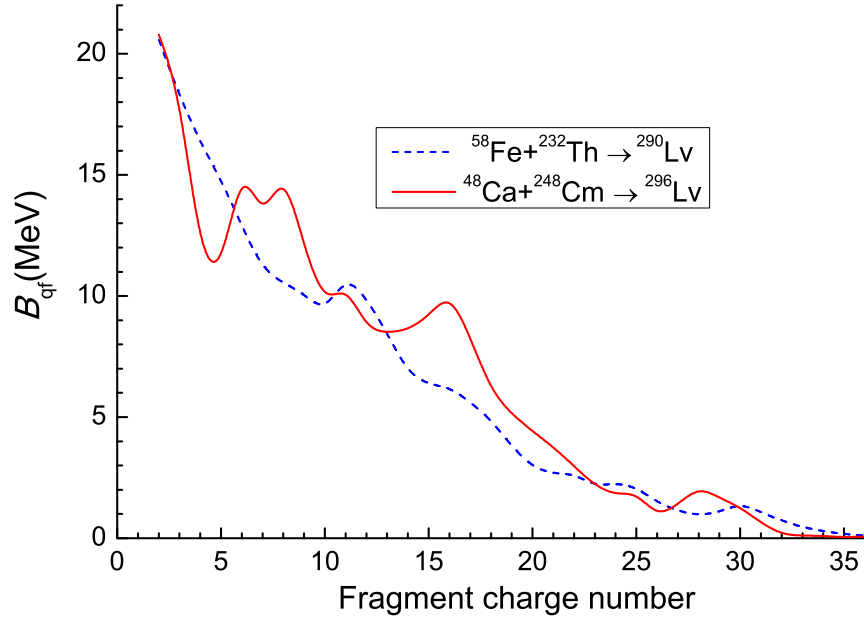


FIG. 5: The quasifission barriers of the DNS fragments as a function of their charge numbers for the  $^{48}\text{Ca}+^{248}\text{Cm}$  (solid curve) and  $^{58}\text{Fe}+^{232}\text{Th}$  (dashed curve) reactions.

transfer occurs (b) if system overcomes intrinsic fusion barrier. Arrow (c) shows one of possibilities of the DNS quasifission. The broken dot-dashed line corresponds to the driving potential  $U(Z, R_m)$  which is determined by the minimum values of the potential wells for each charge value  $Z$ .  $R_m$  is the position of the minimum value of interaction potential on the relative distance  $R$ .

The advantage of hot fusion reactions in comparison with cold fusion reactions is connected with the relatively small hindrance in the stage of CN formation.

In the case of the  $^{58}\text{Fe}+^{232}\text{Th}$  reaction, the value of driving potential corresponding to the initial charge numbers  $Z_P=26$  and  $Z_T=90$  is farther and lower from the fusion barrier placed at  $Z = 9$  (see dashed line in Fig. 4). It is much lower in comparison with that for the  $^{48}\text{Ca}+^{248}\text{Cm}$  reaction. That means the intrinsic fusion barrier for the  $^{58}\text{Fe}+^{232}\text{Th}$  reaction is larger. Furthermore, the quasifission barrier providing relative stability of DNS formed in this reaction is smaller in comparison with that obtained for the  $^{48}\text{Ca}+^{248}\text{Cm}$  reaction. This comparison is presented in Fig. 5. As a result the fusion probability for the  $^{58}\text{Fe}+^{232}\text{Th}$  reaction should be small.

## II. OUTLINE OF THE APPROACH.

We calculate the partial cross section  $\sigma_{ER}^{(\ell)}$  of ER formation after each step  $x$  of the de-excitation cascade after the emission from the hot CN of particles  $\nu(x)n + y(x)p + k(x)\alpha + s(x)$  (where  $\nu(x)$ ,  $y$ ,  $k$ , and  $s$  are numbers of neutrons, protons,  $\alpha$ -particles, and  $\gamma$ -quanta) by formulas (See Refs. [7, 18]):

$$\sigma_{ER}(E_{CN}^*) = \sum_{\ell=0}^{\ell_d} (2\ell + 1) \sigma_{\ell}^{(ER)}(E_{CN}^*), \quad (4)$$

$$\sigma_{\ell}^{(ER)}(E_{CN}^*) = \sigma_{\ell}^{(x-1)}(E_{CN}^*) W_{\text{sur}}^{(x-1)}(E_{CN}^*, \ell), \quad (5)$$

where  $\sigma_{\ell}^{(x-1)}$  is the partial formation cross section of the excited intermediate nucleus of the  $(x - 1)$ th step and  $W_{\text{sur}}^{(x-1)}$  is the survival probability of the  $(x - 1)$ th intermediate nucleus against fission along the de-excitation cascade of CN;  $E_{CN}^* = E_{c.m.} + Q_{gg} - V_{\text{rot}}(\ell)$ ;  $V_{\text{rot}}(\ell)$  is rotational energy of CN;

Due to the dependence of the fission barrier on the angular momentum  $\ell$ , the survival probability  $W_{\text{sur}}(E_{CN}^*, \ell)$  depends on  $\ell$ . The damping of the shell corrections determining the fission barrier is taken into account as in Ref. [17].

If the colliding nuclei are deformed, the possibility of collision with arbitrary orientation angle of their symmetry axis should be considered. Due to the dependencies of the nucleus-nucleus potential ( $V$ ) and moment of inertia for DNS ( $J_R$ ) on the orientation angles of the axial symmetry axis of the deformed nuclei, the excitation function of the capture and fusion are sensitive to the values of orientation angles.

In the case of spherical nuclei we can take into account of the vibrational excitation of their surfaces due to interactions. Here this procedure is used for the projectiles  $^{48}\text{Ca}$  and  $^{64}\text{Ni}$ .

### A. Capture and fusion cross section in collisions of deformed nuclei

The final results of the partial capture and complete fusion cross sections are obtained by averaging the contributions from the different orientation angles  $\alpha_1$  and  $\alpha_2$  (relatively to

the beam direction) of the projectile and target nuclei, respectively [18]:

$$\begin{aligned} \langle \sigma_{\text{fus}}(E_{\text{c.m.}}, \ell) \rangle &= \int_0^{\pi/2} \sin \alpha_1 \int_0^{\pi/2} \sigma_{\text{fus}}(E_{\text{c.m.}}, \ell; \alpha_1, \alpha_2) \\ &\cdot \sin \alpha_2 d\alpha_1 d\alpha_2. \end{aligned} \quad (6)$$

The partial fusion cross section  $\sigma_{\text{fus}}(E_{\text{c.m.}}, \ell; \alpha_1, \alpha_2)$  is determined by the product of the partial capture cross section  $\sigma_{\text{cap}}(E_{\text{c.m.}}, \ell; \alpha_1, \alpha_2)$  and probability  $P_{\text{CN}}$  of the transformation of DNS into CN:

$$\sigma_{\text{fus}}(E, \ell; \alpha_1, \alpha_2) = \sigma_{\text{cap}}(E, \ell; \alpha_1, \alpha_2) P_{\text{CN}}(E, \ell; \alpha_1, \alpha_2). \quad (7)$$

The capture probability and the largest value of orbital angular momentum ( $\ell_d$ ), leading to capture at the given values of the orientation angles  $\alpha_1$  and  $\alpha_2$ , are calculated by solving equations of the relative motion of nuclei. The calculation of capture and fusion cross sections were performed in the framework of the DNS model. The details of this model can be found in Refs. [8, 12, 13, 18].

## B. Including surface vibration of spherical nucleus

The projectiles  $^{48}\text{Ca}$  and  $^{64}\text{Ni}$  are nearly spherical nuclei. In calculations of capture and fusion cross sections the fluctuation of their shape around the spherical shape ( $\beta_\lambda^{(gr)} = 0$ )  $R_P(\theta) = R_P^{(0)}(1 + \sum_{\lambda=2,3} \beta_\lambda P_\lambda(\theta))$  due to the zero-point motion resulting from the quadrupole and octupole excitations is taken into account. We then average the capture and fusion cross sections over the values of the shape parameters used in the calculations:

$$\langle \sigma_i(E_{\text{c.m.}}, \alpha_T) \rangle = \int_{-\beta_2^{(0)}}^{\beta_2^{(0)}} \int_{-\beta_3^{(0)}}^{\beta_3^{(0)}} \sigma_i(E_{\text{c.m.}}; \beta_2^{(P)}, \beta_3^{(P)}, \alpha_T) g(\beta_2^{(P)}, \beta_3^{(P)}) d\beta_2^{(P)} d\beta_3^{(P)}, \quad (8)$$

with  $i = \text{cap}, \text{fus}$  and with the weight function [21]

$$g(\beta_2^{(P)}, \beta_3^{(P)}) = \exp \left[ -\frac{(\sum_\lambda \beta_\lambda^{(P)} Y_{\lambda 0}^*(\alpha_P))^2}{2\sigma_{\beta_P}^2} \right] (2\pi\sigma_{\beta_P}^2)^{-1/2}, \quad (9)$$

where  $\beta_\lambda^{(P)}$  is the current value of the deformation parameters characterizing the shape of the nucleus; for simplicity hereafter, we use  $\beta_P = \{\beta_2^{(P)}, \beta_3^{(P)}\}$  to characterize the parameters of the first collective vibrational states  $2^+$  and  $3^-$ , respectively;  $\alpha_P$  is the direction of the symmetry axis of the projectile shape when it has prolate ( $\beta_2^{(P)} > 0$ ) or oblate ( $\beta_2^{(P)} <$

0) deformation. It is assumed  $\alpha_P = 0$  in our calculations. The dispersion of the shape fluctuations is calculated by the formula

$$\sigma_{\beta_P}^2 = \sum_{n\lambda} \frac{2\lambda + 1}{4\pi} \frac{\hbar}{2D_{n\lambda}\omega_{n\lambda}}, \quad (10)$$

where  $\omega_{n\lambda}$  is the frequency and  $D_{n\lambda}$  is the mass parameter of a collective mode. We use  $n = 1$  and  $\lambda = 2, 3$  for  $^{48}\text{Ca}$  and  $^{64}\text{Ni}$  projectiles.

The amplitudes  $\beta_i^{(m)}$  ( $-\beta_i^{(m)} \leq \beta_i^{(P)} \leq \beta_i^{(m)}$ ,  $i = 2, 3$ ) and the excitation energies  $\hbar\omega_\lambda$  of the first vibrational states  $2^+$  and  $3^-$  are taken from Refs.[22, 23], respectively. The corresponding mass parameter is calculated by formula  $D_\lambda = \hbar/(2\omega_\lambda(\beta_\lambda)^2)$ .

The results obtained by (8) were used in the following formula

$$\langle \sigma_{ER}(E_{c.m.}) \rangle = \int_0^{\pi/2} \sigma_{ER}(E_{c.m.}; \alpha_T) \sin \alpha_T d\alpha_T \quad (11)$$

to calculate the ER cross section by averaging only over the different orientation angles of the symmetry axis  $\alpha_T$  of the deformed target–nucleus. The fusion excitation function is determined by product of the partial capture cross section  $\sigma_{\text{cap}}(E_{c.m.}, \ell)$  and the fusion probability  $P_{CN}$  [24, 25] of DNS at the various  $E_{c.m.}$  values:

$$\sigma_{\text{fus}}(E_{c.m.}; \beta_P, \alpha_T) = \sum_{\ell=0}^{\ell_f} (2\ell + 1) \sigma_{\text{cap}}(E_{c.m.}, \ell; \beta_P, \alpha_T) P_{CN}(E_{c.m.}, \ell; \beta_P, \alpha_T). \quad (12)$$

### C. Quasifission and fast fission of mononucleus evolving to equilibrium shape of compound nucleus

Another binary process which leads to the formation of two fragments similar to that from fusion-fission or quasifission is the fast fission. According to the liquid drop model, the fast fission occurs only at large values of angular momentum  $\ell > \ell_f$  causing disappearance of the macroscopic fission barrier  $B_f(\ell)$  of the rotating nucleus [16]. It is the disintegration of the fast rotating mononucleus, which survives against quasifission (the decay of the DNS into two fragments without formation of the CN), into two fragments.

In the case of very heavy nucleus ( $Z > 106$ ), the fission barrier providing their stability against fission appears only due to shell effects in their binding energy [14, 15]. The damping of the shell effects decreases the possibility of mononucleus to reach the CN equilibrium shape, and the mononucleus breaks down into two fragments without reaching of CN shape.

The fission barrier consists of the contributions of the macroscopic and microscopic parts. The dependence of the fission barrier  $B_{\text{fis}}$  including shell correction  $\delta W$  on the critical angular momentum  $\ell_f$  can be determined by the formula

$$B_{\text{fis}}(\ell, T) = c B_{\text{fis}}^m(\ell) - h(T) q(\ell) \delta W. \quad (13)$$

There is no macroscopic barrier ( $B_{\text{fis}}^m=0$ ) for CN formed in these reactions under discussion. The microscopic (shell) correction to the fission barrier  $\delta W = \delta W_{\text{sad}} - \delta W_{\text{gs}} \simeq -\delta W_{\text{gs}}$  is taken from the table [20, 26–28]. The damping of the microscopic fission barrier on the excitation energy and angular momentum of CN is taken into account by formulas used in Ref. [17]

$$h(T) = \{1 + \exp[(T - T_0)/d]\}^{-1}, \quad (14)$$

and

$$q(\ell) = \{1 + \exp[(\ell - \ell_{1/2})/\Delta\ell]\}^{-1}, \quad (15)$$

where in the formula (14)  $d = 0.3$  MeV and  $T_0 = 1.16$  MeV, and in the formula (15)  $\ell_{1/2} = 20$  and  $\Delta\ell = 3$  values of parameters were used.

The part of the partial fusion cross section with  $\ell > \ell_f$  is considered as partial fast fission cross section. We should stress that for the superheavy elements  $\ell_f$  is not relevant quantity because there is no barrier connected with the liquid drop model. Therefore, in this work we use  $\ell_f$  connected only with the shell corrections.

The fast fission cross section is calculated by summing the contributions of the partial waves corresponding to the range  $\ell_f \leq \ell \leq \ell_d$  leading to the formation of the mononucleus:

$$\sigma_{\text{ff}}(E_{\text{c.m.}}; \beta_P, \alpha_T) = \sum_{\ell_f}^{\ell_d} (2\ell + 1) \sigma_{\text{cap}}(E_{\text{c.m.}}, \ell; \beta_P, \alpha_T) P_{\text{CN}}(E_{\text{c.m.}}, \ell; \beta_P, \alpha_T). \quad (16)$$

The capture cross section in the framework of the DNS model is equal to the sum of the quasifission, fusion-fission, and fast fission cross sections:

$$\sigma_{\text{cap}}^{\ell}(E_{\text{c.m.}}; \beta_P, \alpha_T) = \sigma_{\text{qfiss}}^{\ell}(E_{\text{c.m.}}; \beta_P, \alpha_T) + \sigma_{\text{fus}}^{\ell}(E_{\text{c.m.}}; \beta_P, \alpha_T) + \sigma_{\text{ffis}}^{\ell}(E_{\text{c.m.}}; \beta_P, \alpha_T). \quad (17)$$

It is clear that the fusion cross section includes the cross sections of ERs and fusion-fission products.

Obviously, the quasifission cross section is defined by

$$\sigma_{qfis}(E_{c.m.}; \beta_P, \alpha_T) = \sum_{\ell=\ell_f}^{\ell_d} (2\ell + 1) \sigma_{cap}(E_{c.m.}, \ell; \beta_P, \alpha_T) (1 - P_{CN}(E_{c.m.}, \ell; \beta_P, \alpha_T)), \quad (18)$$

*i.e.* the quasifission process can take place in the whole range of the orbital angular momentum values leading to capture, including central collisions ( $\ell = 0$ ). This is important conclusion since the separation of the ranges of the angular momentum corresponding to the fusion-fission and quasifission products by some critical value  $\ell_{cr}$  in the analysis of the angular distribution of the fissionlike products is doubtful. The results of our calculations show that the ranges of the quasifission and fusion-fission overlap.

### III. COMPARISON OF THE $^{48}\text{Ca}+^{248}\text{Cm}$ AND $^{58}\text{Fe}+^{232}\text{Th}$ REACTIONS LEADING TO SUPERHEAVY ELEMENT Lv

The importance of the charge asymmetry in the CN formation is seen from the comparison of the  $^{48}\text{Ca}+^{248}\text{Cm}$  and  $^{58}\text{Fe}+^{232}\text{Th}$  reactions leading to the  $^{296}\text{Lv}$  and  $^{290}\text{Lv}$  CN, respectively. Fusion excitation functions, which have been obtained for these reactions, are presented by solid line in Figs. 6 and 7, respectively. We stress to main differences: 1) the cross section of the CN formation is larger in the reaction with  $^{48}\text{Ca}$  in comparison with the  $^{58}\text{Fe}+^{232}\text{Th}$  reaction; 2) CN formed in the former reaction has smaller excitation energy.

In Figs. 6 and 7, capture and quasifission cross sections are nearly equal to each other due to the dominant contribution of the quasifission cross section to capture in comparison with the sum of the fast fission and complete fusion.

The number of events going to quasifission increases drastically with the increasing Coulomb interaction and rotational energy in the entrance channel [7, 29]. The Coulomb interaction increases with the increasing charge number of the projectile or target nucleus, as well as it increases with the decreasing charge asymmetry of colliding nuclei at fixed total charge number of DNS. The advantage of the  $^{48}\text{Ca}+^{248}\text{Cm}$  in synthesis of superheavy element is seen already in the CN formation stage.

One can see in Fig. 7 that the fusion excitation function decreases strongly at low energies  $E_{c.m.} < 250$  MeV. This effect is connected with the increase of hindrance to fusion since at these low energies the collisions with small orientation angles ( $\alpha_P$ -projectile and  $\alpha_T$ -target) can only contribute to the CN formation [18, 30]. Collisions with larger orientation

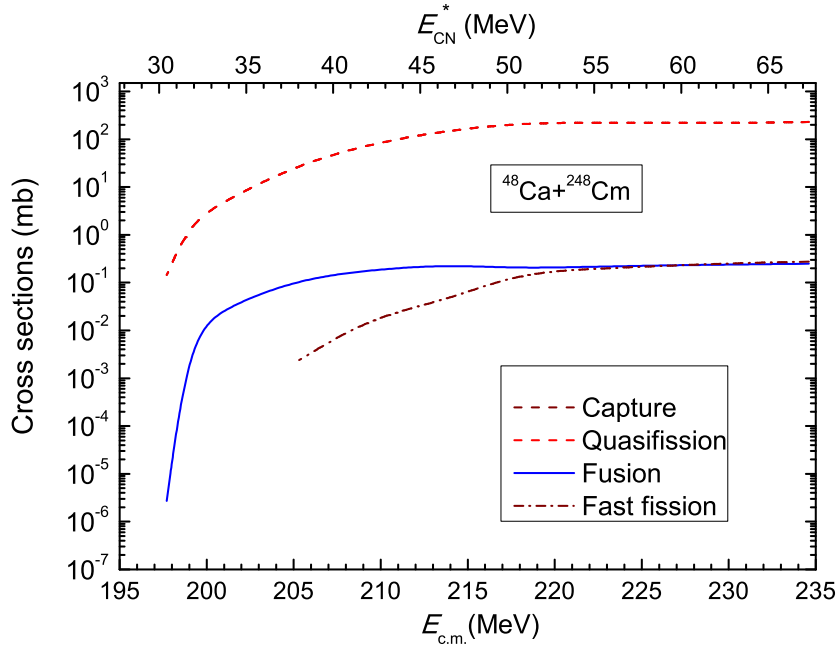


FIG. 6: (Color online) Capture (thin dashed line), quasifission (thick dashed line), fast fission (dot-dashed line) and fusion (solid line) cross sections calculated by the DNS model for the  $^{48}\text{Ca}+^{248}\text{Cm}$  reaction. The excitation energy  $E_{\text{CN}}^*$  of CN (top axis) is calculated by the use of the Möller and Nix mass table [20].

angles  $\alpha_P$  and  $\alpha_T$  can not lead to capture since the beam energy is not enough to overcome the Coulomb barrier of the entrance channel. For the DNS formed in collisions with small orientation angles  $\alpha_P$  and  $\alpha_T$ , the intrinsic fusion barrier  $B_{\text{fus}}^*$  is large [18]. So, the hindrance to complete fusion depends on the orientation angles: more elongated shape of the DNS formed at collisions with small orientation angles (tip-to-tip configurations) promotes the quasifission rather than the formation of the CN [18, 30].

Theoretical results of the ER cross sections for the synthesis of the element  $Z = 116$  are compared with the experimental data in Fig. 8. In this figure, the full triangles and squares show experimental data of the ER cross sections measured in 3n- and 4n-channels, respectively, in the  $^{48}\text{Ca}+^{248}\text{Cm}$  reaction [3]; the curves show theoretical results obtained in this work for the 2n-(solid line), 3n-(dashed line), 4n-(dot-dashed line), and 5n-channel (dotted line) by the DNS and advanced statistical models using the mass tables of Möller and Nix [20] (thin lines) and of Muntian *et al.* [26] (thick lines).

The mass values of the Warsaw group [26] are larger than ones of Möller and Nix [20] by 2-3 MeV for the isotopes of superheavy nuclei with  $Z > 110$  and fission barriers [27, 28] are smaller by 2-3 MeV in comparison with the similar values of Möller and Nix [20]. As a result,

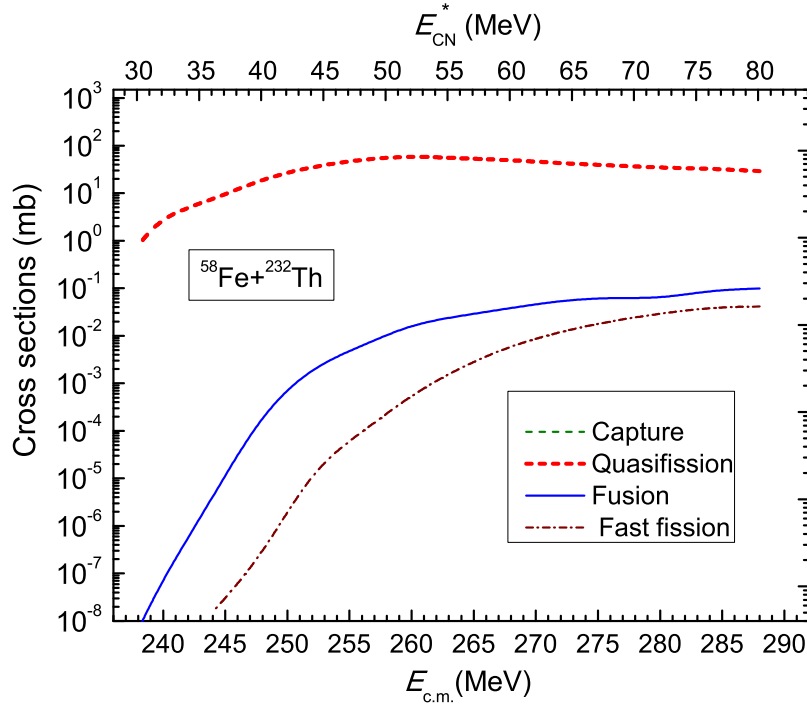


FIG. 7: (Color online) Same as Fig. 6 but for the  $^{58}\text{Fe}+^{232}\text{Th}$  reaction.

the Warsaw group results lead to two main consequences: 1) the excitation energy of the CN ( $E_{\text{CN}}^* = E_{\text{c.m.}} + Q_{\text{gg}}$ ) will be lower since the absolute value of  $Q_{\text{gg}} = B_{\text{proj}} + B_{\text{targ}} - B_{\text{CN}}$  (negative) is larger; 2) the fission probability will be large in comparison with the case of using fission barrier of the Möller and Nix [20] model. When the binding energies and fission barriers of the Warsaw group [26] are used, the total score is that the survival probability  $W_{\text{sur}}$  becomes smaller in comparison with the case of using fission barrier of the Möller and Nix [20] model.

The results of  $\sigma_{\text{ER}}$  for the  $^{48}\text{Ca}+^{248}\text{Cm}$  reaction, calculated by the use of the mass tables of the Warsaw group, better describe the experimental data than the ones obtained by using Möller *et al.* The largest cross section of the yield of superheavy element corresponds to the 4n-channel when the collision energy is in the range  $E_{\text{c.m.}} = 205\text{--}212$  MeV (see Fig. 8).

Concerning the ER formation in the more symmetric  $^{58}\text{Fe}+^{232}\text{Th}$  reaction, the results indicate that this reaction is less favorable in comparison with the  $^{48}\text{Ca}+^{248}\text{Cm}$  reaction to be used in the synthesis of superheavy element  $Z = 116$ . The largest cross section for the 4n-channel is about 1 fb (see Fig. 9) if we use the mass tables of Möller and Nix [20] (thin dot-dot-dashed lines), while the use of the mass table and fission barriers of the Warsaw group leads to smaller cross sections.

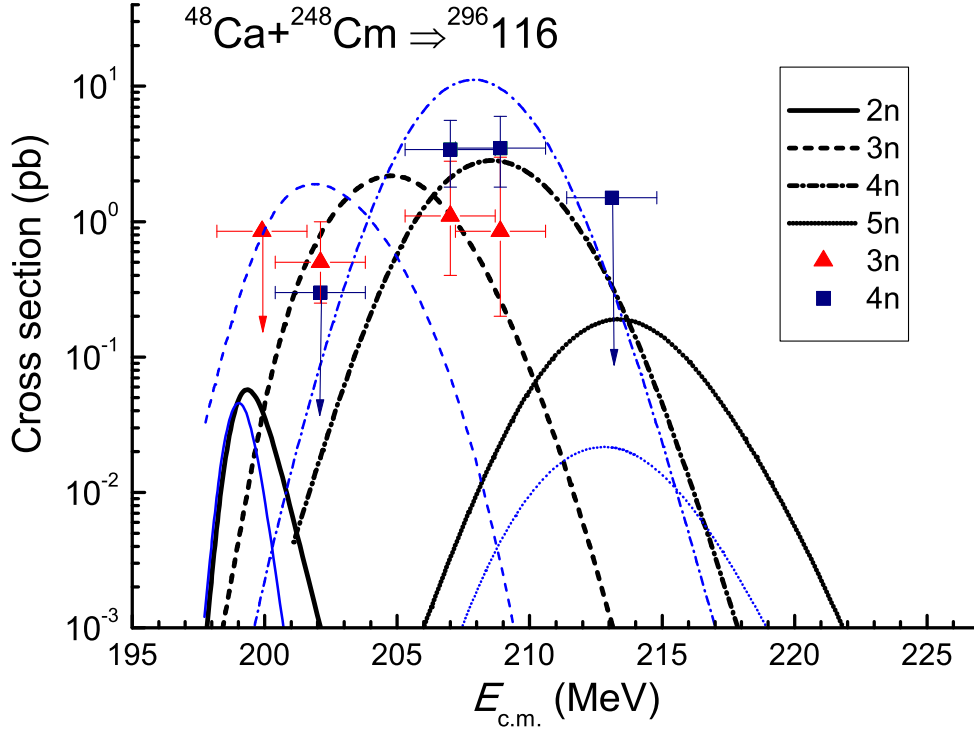


FIG. 8: (Color online) Comparison between the ER excitation functions for the  $^{48}\text{Ca}+^{248}\text{Cm}$  reaction calculated by using mass tables of Möller and Nix [20] (thick lines) and of the Warsaw group [26] (thin lines) for the 2n (solid lines), 3n (dashed lines), 4n (dot-dashed lines), and 5n (dot-dot-dashed lines) channels calculated by the advanced statistical model [31, 32]. The experimental data of Ref. [2, 3] for the 3n and 4n channels are presented by triangles and squares, respectively.

#### IV. COMPARISON OF $^{48}\text{Ca}+^{249}\text{Cf}$ AND $^{64}\text{Ni}+^{232}\text{Th}$ REACTIONS LEADING TO SUPERHEAVY ELEMENT $Z=118$

The dynamics of the capture and fusion for the  $^{48}\text{Ca}+^{249}\text{Cf}$  and  $^{64}\text{Ni}+^{232}\text{Th}$  reactions leading to  $Z = 118$  differs significantly since the values of the Coulomb parameter  $z = Z_1 \cdot Z_2 / (A_1^{1/3} + A_2^{1/3})$  are very different, 197.47 and 248.41 for the reaction with Ca and Ni, respectively. As shown in the systematic analysis [25] at values  $z > 240$ , the fusion probability  $P_{\text{CN}}$  becomes less than  $10^{-7}$ . The measured smallest value of ER cross section is 50 fb [1] in the cold fusion  $^{70}\text{Zn}+^{209}\text{Bi}$  reaction which has the Coulomb parameter  $z = 247.62$ . It is very close to the value for the reaction with Ni in our case. The capture, quasifission, fusion, and fast fission cross sections calculated in this work for the  $^{48}\text{Ca}+^{249}\text{Cf}$  and  $^{64}\text{Ni}+^{232}\text{Th}$  reactions are presented in Figs. 10 and 11, respectively.

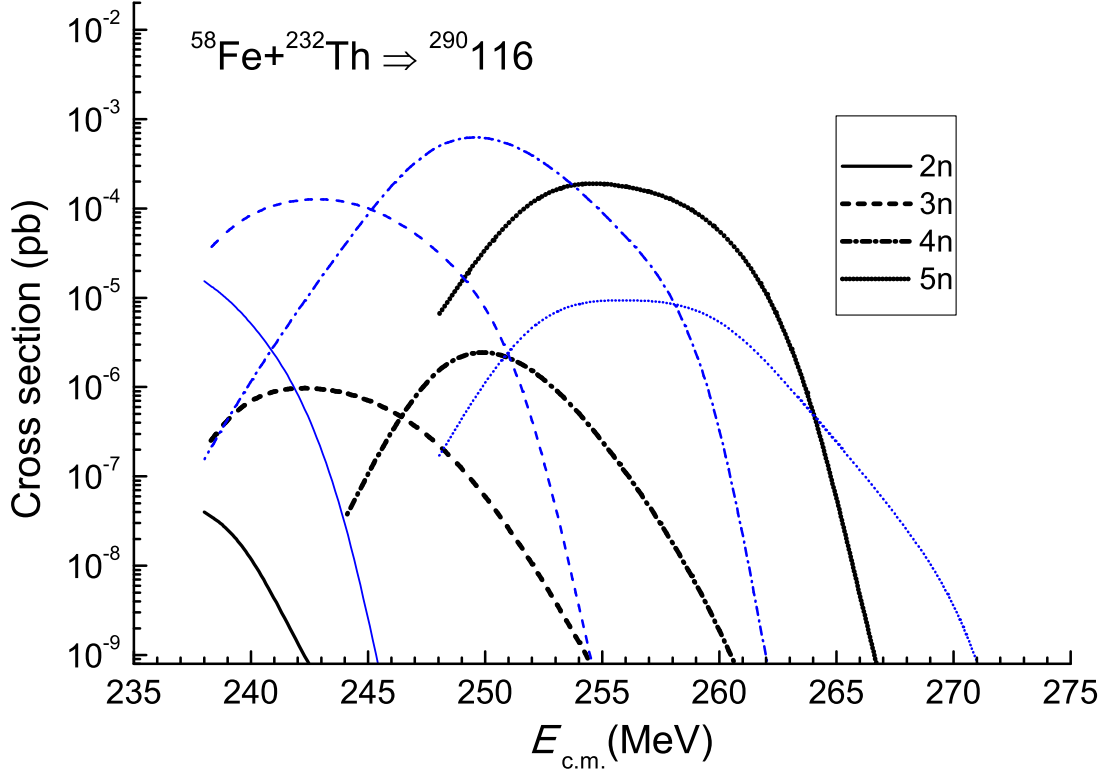


FIG. 9: (Color online) The same as in Fig. 8 but for the  $^{58}\text{Fe}+^{232}\text{Th}$  reaction.

As we have stressed in Section III, in these reactions with massive nuclei, the capture and quasifission cross sections are equal since the sum of the fast fission and complete fusion is much smaller than the quasifission cross section.

The comparison between these figures shows that, at low energies, the capture cross section in the  $^{64}\text{Ni}+^{232}\text{Th}$  reaction is much smaller than that in the  $^{48}\text{Ca}+^{249}\text{Cf}$  reaction, while these cross sections become comparable at larger energies. The smallness of capture cross section is connected with the shallow potential well in the nucleus-nucleus interaction for the collisions with small orientation angles since the Coulomb interaction is stronger for more symmetric reactions. At low energies the projectile can overcome the Coulomb barrier for collisions with small orientation angles.

One can also see in these figures that the fusion cross section is sufficiently large for the  $^{48}\text{Ca}+^{249}\text{Cf}$  reaction in comparison with the one of the  $^{64}\text{Ni}+^{232}\text{Th}$  reaction.

The advantage of the charge asymmetric system in complete fusion appears at the second stage (fusion) of the reaction mechanism leading to the ER formation. It is well known that the hindrance to complete fusion decreases with the increasing DNS charge asymmetry. At

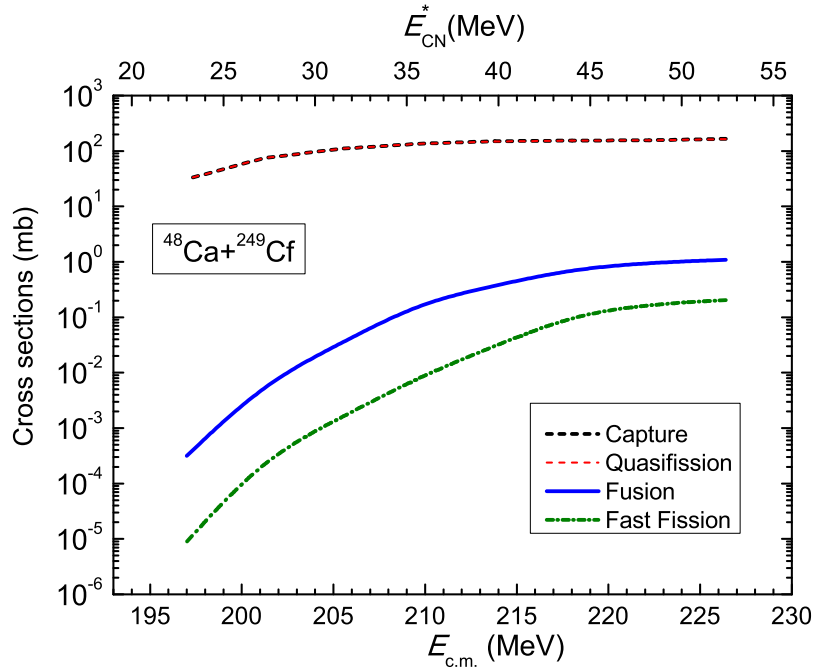


FIG. 10: (Color online) Quasifission (dashed line), fast fission (dot-dashed line), and complete fusion (solid line) excitation functions calculated by the DNS model [8, 18, 29] for the  $^{48}\text{Ca}+^{249}\text{Cf}$  reaction which could lead to the  $^{297}118$  CN. The capture cross section is not shown here because it is completely overlapped with the quasifission cross section. The excitation energy  $E_{\text{CN}}^*$  (top axis) is calculated by the use of the Möller and Nix mass table [20].

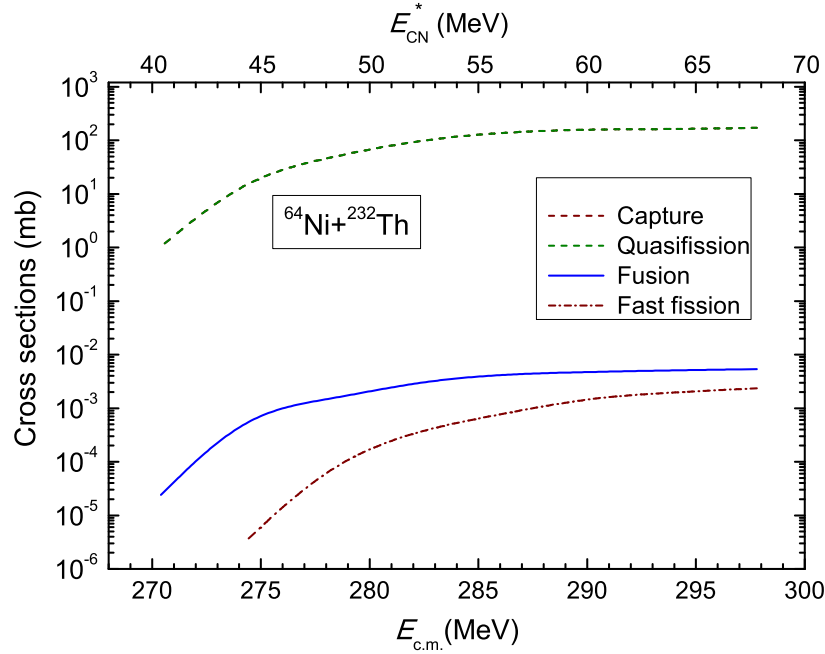


FIG. 11: (Color online) Same as in Fig. 10 but for the  $^{64}\text{Ni}+^{232}\text{Th}$  reaction.

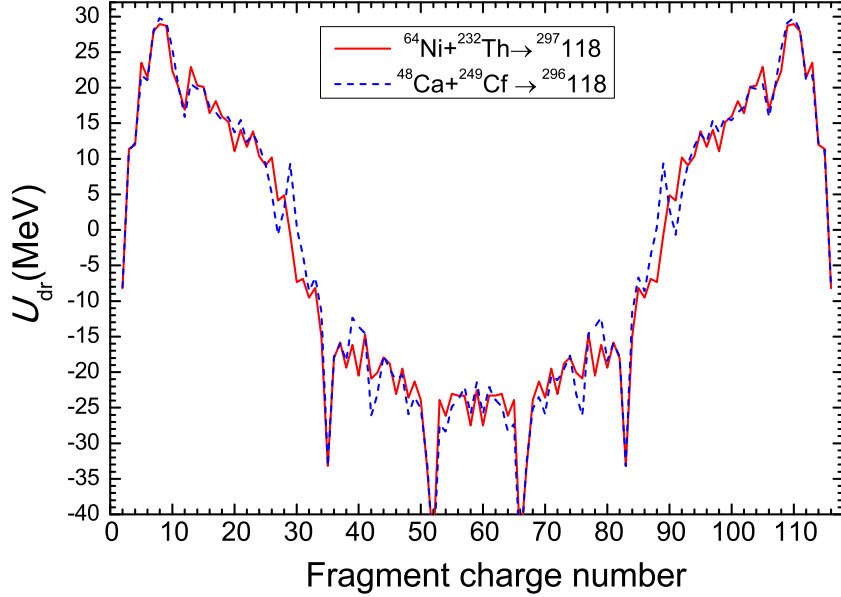


FIG. 12: (Color online) Comparison of the driving potentials calculated for the DNS formed in the  $^{48}\text{Ca}+^{249}\text{Cf}$  and  $^{64}\text{Ni}+^{232}\text{Th}$  reactions which can lead to formation of isotopes  $A=297$  and  $296$  of new superheavy element  $Z=118$  as a function of the fragment charge number.

the same time the DNS quasifission barrier,  $B_{\text{qf}}$ , increases since the Coulomb repulsion forces decrease with the decrease of the product  $Z_1 \cdot Z_2$ . The stronger hindrance to complete fusion in the case of the  $^{64}\text{Ni}+^{232}\text{Th}$  reaction is connected with the larger intrinsic fusion barrier  $B_{\text{fus}}^*$  (see Fig. 12) and smaller quasifission barrier  $B_{\text{qf}}$  for this reaction in comparison with  $^{48}\text{Ca}+^{249}\text{Cf}$  (see Fig. 13). These two reasons mainly lead smaller fusion probability for the  $^{64}\text{Ni}+^{232}\text{Th}$  reaction.

The theoretical ER excitation functions which can be formed in different neutron-emission channels for these two systems are presented in Figs. 14 and 15. In each of the figures the evaporation residue cross sections for the neutron-emission channels obtained by using binding energies and fission barriers calculated in the microscopic-macroscopic models of Möller and Nix [20] and of the Warsaw group [26] are compared.

In Fig. 14, we present the results for the  $^{48}\text{Ca}+^{249}\text{Cf}$  reaction [17] leading to  $^{297}118$  CN to compare with the results calculated for the  $^{64}\text{Ni}+^{232}\text{Th}$  reaction leading to the same superheavy element  $^{296}118$  with smaller mass number. In the  $^{48}\text{Ca}+^{249}\text{Cf}$  experiment (see Ref. [3]) the superheavy element  $^{294}118$  was observed after emission of three neutrons from the  $^{297}118$  CN, at two projectile energies corresponding to  $E_{\text{CN}}^*=29.2$  and  $34.4$  MeV. As seen in Fig. 14 the maximum values of cross sections connected with the 2n, 3n, and 4n emission

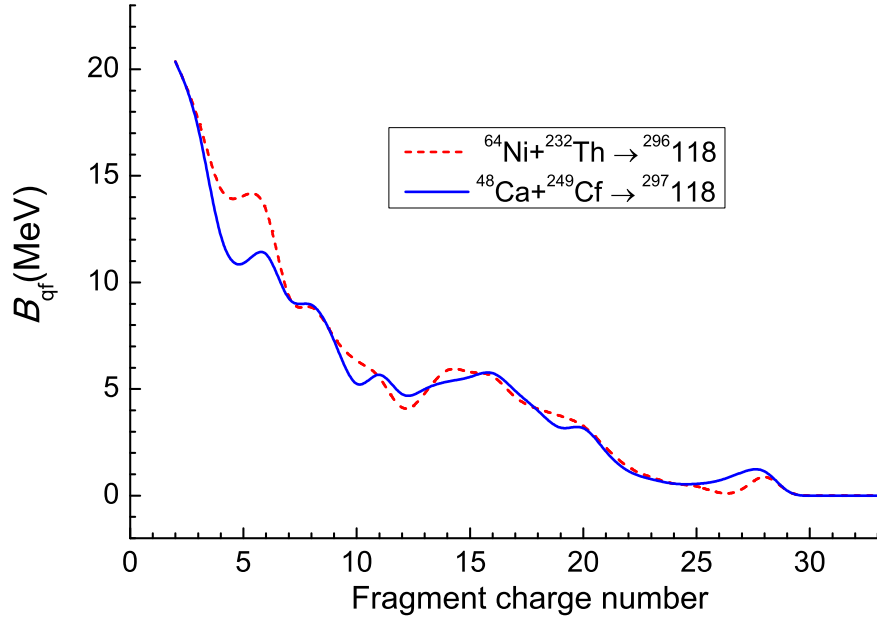


FIG. 13: The quasifission barriers of the DNS fragments as a function of their charge numbers for the  $^{48}\text{Ca}+^{249}\text{Cf}$  (solid curve) and  $^{64}\text{Ni}+^{232}\text{Th}$  (dashed curve) reactions.

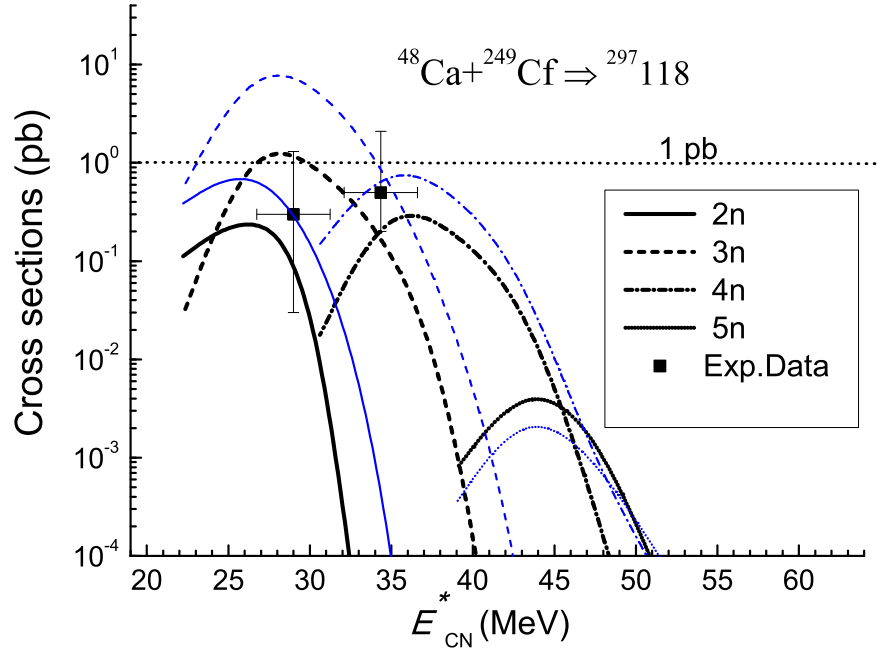


FIG. 14: (Color online) Comparison between the ER excitation functions for the  $^{48}\text{Ca}+^{249}\text{Cf}$  reaction calculated by using mass tables of Möller and Nix [20] (thin lines) and of the Warsaw group [26] (thick lines) for the 2n (dashed lines), 3n (solid lines), 4n (dot-dashed lines), and 5n (dotted lines) channels calculated by the advanced statistical model [31, 32]. The experimental data of Ref. [3] are presented by squares.

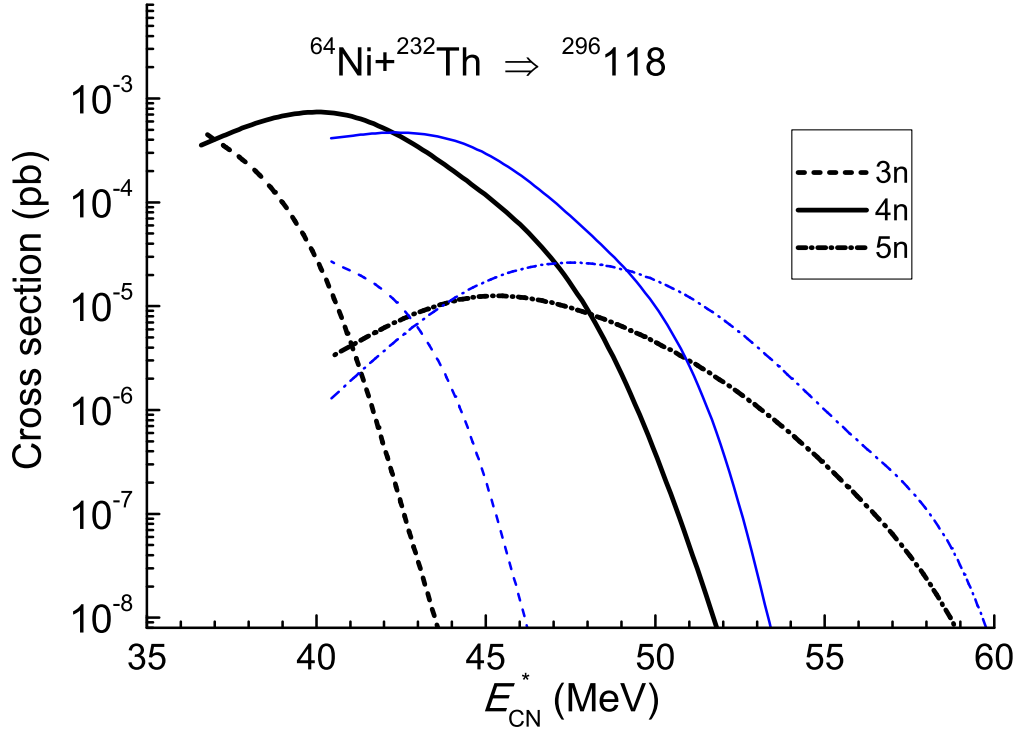


FIG. 15: (Color online) Same as in Fig. 14 but for the  $^{64}\text{Ni}+^{232}\text{Th}$  reaction.

channels are in the range between 0.3 pb and 1.2 pb.

One can see from Fig. 15 that the results obtained for all  $xn$ -channels of ER formation in the  $^{64}\text{Ni}+^{232}\text{Th}$  reaction are very small. The largest point of the 4n-channel curve is less than 1 fb. That means this reaction is not favorable to obtain any isotopes of the superheavy element 118.

## V. CONCLUSIONS

In the framework of the combined DNS and advanced statistical models, the ER excitation functions have been calculated for the  $^{48}\text{Ca}+^{248}\text{Cm}$  and  $^{58}\text{Fe}+^{232}\text{Th}$  reactions leading to new superheavy element Lv ( $Z=116$ ) and the  $^{48}\text{Ca}+^{249}\text{Cf}$  and  $^{64}\text{Ni}+^{232}\text{Th}$  reactions leading to new superheavy element  $Z=118$ . The results obtained in this work are compared with the experimental data given in Refs. [2, 3]. The ER excitation functions of the 3n- and 4n-channels for the  $^{48}\text{Ca}+^{248}\text{Cm}$  reaction are well described when the Muntian *et al.* [26] mass tables are used, while in both cases the use of the Möller and Nix [20] mass tables leads to overestimation of the experimental data.

The results of the ER excitation functions for the  $^{58}\text{Fe}+^{232}\text{Th}$  reaction indicate that this reaction is less favorable to be used in the synthesis of superheavy element  $Z = 116$ . The largest cross section for the 4n-channel is about 1 fb (see Fig. 9), if we use the mass tables of Möller and Nix [20] (thin dash-dotted lines), while the use of the mass table and fission barriers of Warsaw group leads to much lower cross sections. The modern state of the experimental setup does not allow to observe these events.

The reactions with the  $^{232}\text{Th}$  target and  $^{58}\text{Fe}$  and  $^{64}\text{Ni}$  projectiles can be useful to study the role of the entrance channel and nuclear structure in formation of the fusion-fission and quasifission products. From the comparison of Figs. 6 and 7 we can state that the fusion excitation function for the  $^{58}\text{Fe}+^{232}\text{Th}$  reaction is from  $10^{-5}$  to  $10^{-2}$  orders lower than the one calculated for the  $^{48}\text{Ca}+^{248}\text{Cm}$  reaction depending on the beam energy. The strong hindrance at low energies is caused by the large intrinsic fusion barrier  $B_{\text{fus}}^*$  for the small orientation angles of the symmetry axis of the deformed projectile  $^{58}\text{Fe}$  ( $\beta_2 = 0.2$ ) and target  $^{232}\text{Th}$  ( $\beta_2 = 0.26$ ) nuclei. Therefore, the curve of the fusion excitation function increases slightly with the increasing the beam energy.

### Acknowledgments

A. K. Nasirov is grateful to the Rare Isotope Science Project of the Institute for Basic Science of the Republic of Korea for the support the collaboration between the Dubna and Daejeon groups, and he thanks the Russian Foundation for Basic Research for the partial financial support in the performance of this work. The work of Y. Kim and K. Kim was supported by the Rare Isotope Science Project funded by the Ministry of Science, ICT and Future Planning (MSIP) and National Research Foundation (NRF) of Korea.

- 
- [1] Kosuke Morita, Kouji Morimoto, Daiya Kaji, Takahiro Akiyama, Sin-ichi Goto, Hiromitsu Haba, Eiji Ideguchi, Rituparna Kanungo, Kenji Katori, Hiroyuki Koura, Hisaaki Kudo, Tetsuya Ohnishi, Akira Ozawa, Toshimi Suda, Keisuke Sueki, HuShan Xu, Takayuki Yamaguchi, Akira Yoneda, Atsushi Yoshida and YuLiang Zhao, *J. Phys. Soc. Japan*, **76**, 043201 (2007).
- [2] Yu. Ts. Oganessian, V. K. Utyonkov, Yu. V. Lobanov, F. Sh. Abdullin, A. N. Polyakov, I. V. Shirokovsky, Yu. S. Tsyganov, G. G. Gulbekian, S. L. Bogomolov, B. N. Gikal, A. N. Mezentsev, S. Iliev, V. G. Subbotin, A. M. Sukhov, A. A. Voinov, G. V. Buklanov, K. Subotic,

- V. I. Zagrebaev, and M. G. Itkis, J. B. Patin, K. J. Moody, J. F. Wild, M. A. Stoyer, N. J. Stoyer, D. A. Shaughnessy, J. M. Kenneally, P. A. Wilk, and R. W. Lougheed, R. I. Il'kaev and S. P. Vesnovskii, *Phys. Rev. C* **70**, 064609 (2004).
- [3] Yu. Ts. Oganessian, V. K. Utyonkov, Yu. V. Lobanov, F. Sh. Abdullin, A. N. Polyakov, R. N. Sagaidak, I. V. Shirokovsky, Yu. S. Tsyganov, A. A. Voinov, G. G. Gulbekian, S. L. Bogomolov, B. N. Gikal, A. N. Mezentsev, S. Iliev, V. G. Subbotin, A. M. Sukhov, K. Subotic, V. I. Zagrebaev, G. K. Vostokin, and M. G. Itkis, K. J. Moody, J. B. Patin, D. A. Shaughnessy, M. A. Stoyer, N. J. Stoyer, P. A. Wilk, J. M. Kenneally, J. H. Landrum, J. F. Wild, and R. W. Lougheed, *Phys. Rev. C* **74**, 044602 (2006).
- [4] L. Stavsetra, K. E. Gregorich, J. Dvorak, P. A. Ellison, I. Dragojević, M. A. Garcia, and H. Nitschel, *Phys. Rev. C* **103**, 132502 (2009).
- [5] J. M. Gates, Ch. E. Düllmann, M. Schadel, A. Yakushev, A. Turler, K. Eberhardt, J. V. Kratz, D. Ackermann, L.-L. Andersson, M. Block, W. Bruchle, J. Dvorak, H. G. Essel, P. A. Ellison, J. Even, U. Forsberg, J. Gellanki, A. Gorshkov, R. Graeger, K. E. Gregorich, W. Hartmann, R.-D. Herzberg, F. P. Heßberger, D. Hild, A. Hubner, E. Jäger, J. Khuyagbaatar, B. Kindler, J. Krier, N. Kurz, S. Lahiri, D. Liebe, B. Lommel, M. Maiti, H. Nitsche, J. P. Omtvedt, E. Parr, D. Rudolph, J. Runke, H. Schaffner, B. Schausten, E. Schimpf, A. Semchenkov, J. Steiner, Th. Th. Pospiech, J. Uusitalo, M. Wegrzecki, and N. Wieh, *Phys. Rev. C* **83**, 054618 (2011).
- [6] S. Hofmann, S. Heinz, R. Mann, J. Maurer, J. Khuyagbaatar, D. Ackermann, S. Antalic, W. Barth, M. Block, H.G. Burkhard, V.F. Comas, L. Dahl, K. Eberhardt, J. Gostic, R.A. Henderson, J.A. Heredia, F.P. Heßberger, J.M. Kenneally, B. Kindler, I. Kojouharov, J.V. Kratz, R. Lang, M. Leino, B. Lommel, K.J. Moody, G. Münzenberg, S.L. Nelson, K. Nishio, A.G. Popeko, J. Runke, S. Saro, D.A. Shaughnessy, M.A. Stoyer, P. Th. Th. Pospiech, K. Tinschert, N. Trautmann, J. Uusitalo, P.A. Wilk, and A.V. Yeremin, *Eur. Phys. J. A* **48**, 62 (2012).
- [7] G. Giardina, S. Hofmann, A. I. Muminov, A. K. Nasirov, *Eur. Phys. J. A* **8** 205 (2000).
- [8] G. Fazio, G. Giardina, G. Mandaglio, F. Hanappe, A. I. Muminov, A. K. Nasirov, W. Scheid, L. Stuttgé, *Mod. Phys. Lett. A* **20**, 391 (2005).
- [9] B. B. Back, R. R. Betts, J. E. Gindler, B. D. Wilkins, and S. Saini, M. B. Tsang, C. K. Gelbke, and W. G. Lynch, M. A. McMahan, and P. A. Baisden, *Phys. Rev. C* **32**, 195 (1985).

- [10] N. V. Antonenko, E. A. Cherepanov, A. K. Nasirov, V. P. Permjakov, V. V. Volkov, *Phys. Lett B* **319** 425 (1993); *Phys. Rev. C* **51**, 2635 (1995).
- [11] G.G. Adamian, N.V. Antonenko, W. Scheid, *Phys. Rev. C* **68**, 034601 (2003).
- [12] G. Fazio, G. Giardina, A. Lamberto, R. Ruggeri, C. Saccà, R. Palamara, A. I. Muminov, A. K. Nasirov, U. T. Yakhshiev, F. Hanappe, *Eur. Phys. J. A* **19**, 89 (2004).
- [13] A. K. Nasirov, G. Giardina, G. Mandaglio, and M. Manganaro, F. Hanappe, S. Heinz and S. Hofmann, A. I. Muminov, W. Scheid, *Phys.Rev. C* **79**, 024606 (2009).
- [14] Peter Armbruster, *Ann. Rev. Nucl. Part. Sci.* **35** (1985) 135.
- [15] A. Sobiczewski, K. Pomorski, *Prog. Part. Nucl. Phys.* **58**, 292 (2007).
- [16] A.J. Sierk: *Phys. Rev. C* **33** (1986) 2039.
- [17] G. Mandaglio, G. Giardina, A. K. Nasirov, and A. Sobiczewski, *Phys. Rev. C* **86**, 064607 (2012).
- [18] Avazbek Nasirov, Akira Fukushima, Yuka Toyoshima, Yoshihiro Aritomo, Akhtam Muminov, Shuhrat Kalandarov, Ravshanbek Utamuratov, *Nucl. Phys. A* **759**, 342 (2005).
- [19] G. Audi, A.H. Wapstra, *Nucl. Phys.* **A595** (1995) 509.
- [20] P. Möller and J.R. Nix, *J. Phys. G: Nucl. Part. Phys.* **20**, 1681 (1994).
- [21] H. Esbensen: *Nucl. Phys. A* **352** (1981) 147.
- [22] S. Raman, C.H. Malarkey, W.T. Milner, C.W. Nestor, Jr., and P.H. Stelson: *Atomic Data and Nuclear Data Tables* **36** (1987) 1.
- [23] R. H. Spear: *Atomic Data and Nuclear Data Tables* **42**, No. 1 (1989) 55.
- [24] A. K. Nasirov, A. I. Muminov, R. K. Utamuratov, G. Fazio, G. Giardina, F. Hanappe, G. Mandaglio, M. Manganaro, and W. Scheid: *Eur. Phys. J. A* **34** (2007) 325.
- [25] G. Giardina, A K Nasirov, G Mandaglio, F Curciarello, V De Leo, G Fazio, M Manganaro, M Romaniuk, C Saccá, *Jour. of Physics: Conference Series* **282**, 012006 (2011)
- [26] I. Muntian, Z. Patyk, and A. Sobiczewski, *Phys. At. Nuclei* **66**, 1015 (2003).
- [27] M. Kowal, P. Jachimowicz, and A. Sobiczewski, *Phys. Rev. C* **82**, 014303 (2010).
- [28] M. Kowal and A. Sobiczewski, *Int. J. Mod. Phys. E* **18**, 914 (2009).
- [29] G. Fazio, G. Giardina, G. Mandaglio, R. Ruggeri, A. I. Muminov, A. K. Nasirov, Yu. Ts. Oganessian, A. G. Popeko, R. N. Sagaidak, A. V. Yeremin, S. Hofmann, F. Hanappe, C. Stodel, *Phys.Rev. C* **72** 064614 (2005).
- [30] D.J. Hinde, M. Dasgupta, J.R. Leigh, J.P. Lestone, J.C.Mein, C.R.Morton, J.O. Newton, H.

- Timmers, Phys. Rev. Lett. **74**, 1295 (1995).
- [31] A. D'Arrigo, G. Giardina, M. Herman, and A. Taccone, Phys. Rev. C **46**, 1437 (1992).
- [32] R. N. Sagaidak, V. I. Chepigin, A. P. Kabachenko, J. Rohac, Yu. Ts. Oganessian, A. G. Popeko, A. A. Yeremin, A. D'Arrigo, G. Fazio, G. Giardina, M. Herman, R. Ruggeri, and R. Sturiale, J. Phys. G **24**, 611 (1998).